Ultralow-field nuclear magnetic resonance of liquids confined in ferromagnetic and paramagnetic materials

Michael C. D. Tayler,[1,2,a] Jordan Ward-Williams,[1] and Lynn F. Gladden[1]
[1] *Department of Chemical Engineering and Biotechnology, University of Cambridge, Cambridge CB3 0AS, United Kingdom*
[2] *ICFO – The Institute of Photonic Sciences, Castelldefels (Barcelona), 08860, Spain*

(Dated: July 8th, 2019)

ABSTRACT

A nuclear magnetic resonance (NMR) procedure is used to measure weak magnetic fields in the vicinity of dilute ferromagnetic and/or paramagnetic materials. By detecting ^{1}H Larmor precession in common solvents at extremely low frequencies (<50 Hz), the magnetic field produced by remanent magnetization of the material is measured by NMR to a precision of <1 nT. In one example, the technique is used to quantify the magnitude and direction of remanent magnetization in a common aluminum alloy. In another example, a ^{1}H NMR line width <1 Hz is demonstrated for liquid decane (n-$C_{10}H_{22}$) imbibed inside a mesoporous silica matrix, despite a high concentration of paramagnetic cobalt sites that produce magnetic susceptibility gradients in the system. Application to systems of industrial relevance is discussed.

MAIN TEXT

Nuclear magnetic resonance (NMR) techniques provide unique physical and chemical insights into the behavior of fluids, including detail on composition, dynamics and reactivity. Furthermore, such insights are permitted even when the fluid is enclosed in a structure that is opaque to visible radiation, in particular *in vivo*[1] and in porous nanomaterials[2]. However, for many reasons, metallic systems remain a technical challenge. The spatial and spectroscopic resolution of NMR near metals can be obstructed by induced gradients in the applied magnetic field, caused by magnetic susceptibility changes at the material boundary[3–6] and ferromagnetism. Furthermore, due to high electrical conductivity, eddy currents limit the penetration depth of radiofrequency NMR signals. It is becoming established, however, that these problems can be mitigated by detecting NMR at a sufficiently low magnetic field strength. Induced gradients scale linearly with field strength[7], while skin depth scales with the inverse square root of the NMR signal frequency[8,9]. In copper or aluminum, for example, the skin penetration depth exceeds several mm at the ^{1}H Larmor frequency in the earth's field (∼2 kHz, ∼50 μT). So far, NMR in the μT to mT range has been used to study fluids enclosed inside porous metals[10,11], pipes[12] and metal food/beverage cans[13,14], predominantly using superconducting quantum interferences devices[15–22] or alkali vapor magnetometers[23–31] as efficient low-frequency detectors of nuclear precession.

This Letter reports on ultralow-field NMR of liquids enclosed in sample vessels or nanoscale confinement that are weakly ferromagnetic (i.e. have a magnetic moment even at zero applied field) and/or paramagnetic (i.e. have a magnetic moment proportional to the applied field). Both types of magnetism may contribute to the net field experienced by the nuclear spins, resulting in frequency shifts or broadening the NMR spectral line that distinguish each type of contribution.

The experimental setup is illustrated in Fig. 1. The NMR sample to be studied is placed in a container of up to 12.7 mm diameter and positioned adjacent to a spin-exchange relaxation-free[32] rubidium magnetometer (^{87}Rb in a $5 \times 5 \times 8$ mm^3 glass cuboid cell, 150 °C, noise floor <20 fT/$\sqrt{\text{Hz}}$, bandwidth ∼200 Hz). The magnetometer employs two laser beams propagating along the x and y axes (794.97 nm circularly polarized beam along x, for optical pumping; 795.12 nm linearly polarized probing beam along y) to detect, via the magneto-optical rotation in the probe beam[27], the component of total magnetic field along the z axis. Two electromagnetic coils also surround the container and magnetometer, one oriented along the z axis to pre-polarize the nuclei in the sample

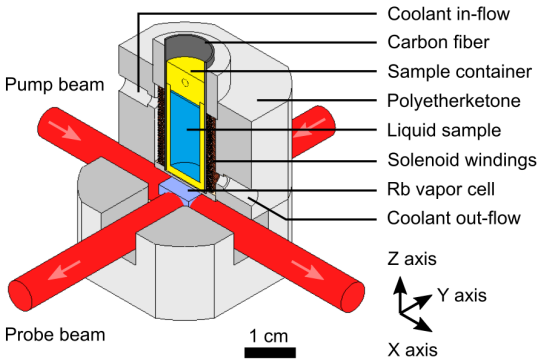

FIG. 1. Experimental setup for ultralow-field NMR, showing solenoid coil for nuclear spin prepolarization and ^{87}Rb atomic magnetometer used to detect the NMR signals.

[a] Electronic mail: michael.tayler@icfo.eu

(30 mT/A 8-layer end-compensated solenoid, American gauge 31 enameled Cu wire, air cooled) and the other along the x axis (saddle coil, 130 mm diameter, 80 μT/A to within 2000 ppm/cm) to provide a magnetic field B_x for nuclear precession. The assembly shown in Fig. 1 is placed inside a Mu-metal chamber (Twinleaf LLC model MS-1F) to passively shield out the laboratory magnetic field to below 1 nT. Nuclear magnetization is created by supplying electric current to the polarizing coil. After non-adiabatically switching off the polarizing coil (<0.1 ms) the magnetization precesses in the yz plane at the nuclear Larmor frequency[33] and the vector component along z is transduced by the magnetometer into an AC voltage signal. The signal is digitally sampled in the time domain (4 s, 16 bit, 4000 samples/s, with AC coupling) then Fourier transformed to yield the spectrum. If the total magnetic bias field comprises only the applied term B_x, i.e. $\boldsymbol{B} = (B_x, 0, 0)$, the spectrum of a ^{1}H-containing sample should yield the nuclear precession signal at a frequency

$$|\nu_{\rm H}| = |\gamma_{\rm H} B_x|/2\pi, \qquad (1)$$

(in Hz), where $\gamma_{\rm H}/2\pi = 42.576$ Hz/μT is the ^{1}H gyromagnetic ratio. If, additionally, the sample produces a bias field $\boldsymbol{\delta B} = (\delta B_x, \delta B_y, \delta B_z)$ where $|\boldsymbol{\delta B}| \ll |\boldsymbol{B}|$, then

$$|\nu_{\rm H}| \approx |\gamma_{\rm H}(B_x + \delta B_x + \boldsymbol{\delta B}\cdot\boldsymbol{\delta B}/2B_x)|/2\pi. \qquad (2)$$

The term $\boldsymbol{\delta B}\cdot\boldsymbol{\delta B}/2B_x$ in Eq. 2 is negligible compared to δB_x. Therefore, ν_H is primarily sensitive to magnetic fields parallel to $\boldsymbol{B}$.

We start by demonstrating a nonzero term $\boldsymbol{\delta B}$ arising from the sample container via the example of 1.5 cm^3 de-mineralized H_2O encased in a closed cylindrical vessel made of either Ketron polyether-ether-ketone/PEEK (dashed curve) or aluminum alloy 6082-T6 (solid curve). Aluminum alloy 6082-T6 (>95% Al) is a common engineering material used in high-stress applications; it is easily wrought, machined and has the highest strength of the 6000 aluminum series. Dimensions of the containers are shown in Fig. 2a. Corresponding ^{1}H precession spectra were acquired by applying a polarization field of 20 mT for 4 s prior to a detection field of $B_x = 0.9395$ μT ($|\nu_{\rm H}| = 40.0$ Hz), see Fig. 2b.

The striking result in Fig. 2b is the different frequency of ^{1}H precession in the two containers, despite the same applied field B_x. In the PEEK container $\nu_{\rm H} = 40.0$ Hz is measured and corresponds to the frequency expected via Eq. 1. In the aluminum container the ^{1}H frequency is shifted by more than 1 Hz. In an attempt to understand the origin of the shift, another set of data were recorded at a field $B_x = 0.587$ μT; here, the frequency $\nu_{\rm H}$ was measured for different orientations of the container with respect to B by rotating the sample container about the z axis (45° angular increments). In this way, the coarse dependence of $\nu_{\rm H}$ versus δB_x and δB_y was obtained. As shown in Fig. 3, the experimental data fit to a curve $|\nu_{\rm H}(\varphi)| = |\gamma_{\rm H}(B_x + \Delta B\cos\varphi)/(2\pi)|$ (dotted line), where

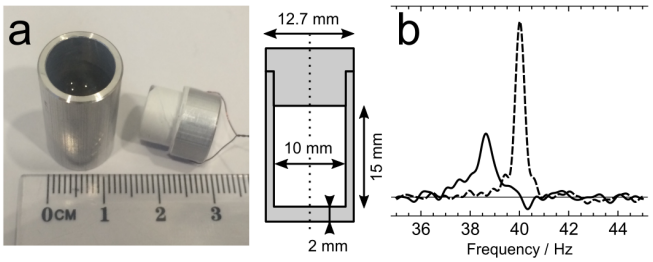

FIG. 2. (a) Photograph and dimensions of the sample container, internal volume 1.5 cm^3; (b) NMR spectra at $B_x = 0.9395$ μT for de-mineralized H_2O in PEEK (dashed line) or aluminum (solid line) containers, average of 64 scans.

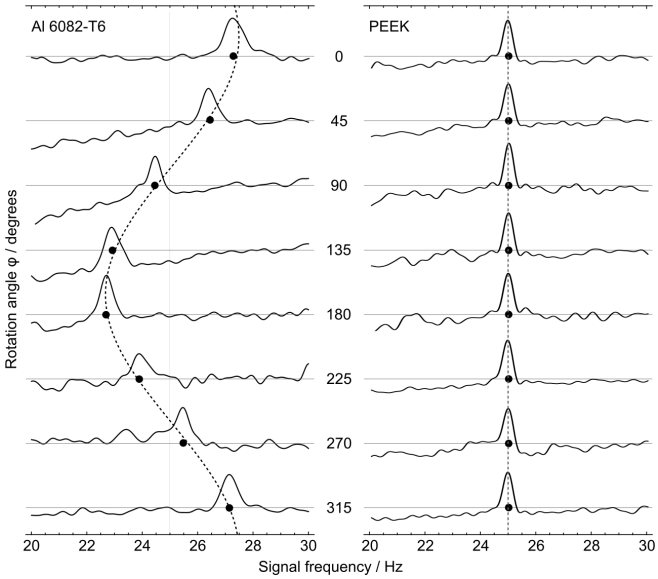

FIG. 3. Fourier-transform ^{1}H NMR spectra of 1.5 cm^3 water inside the cylindrical aluminum and PEEK containers, showing dependence on rotation angle about the z axis.

$\gamma_{\rm H}B_x/(2\pi) = 25.00$ Hz is the ^{1}H Larmor frequency in the applied field $B_x = 0.587$ μT, $\Delta B = (54.7 \pm 1.0)$ nT is the strength of the orientation-dependent magnetic field and φ is the rotation angle, which may defined through $\delta B_x = \Delta B\cos\varphi$ and $\delta B_y = \Delta B\sin\varphi$ to within a constant.

The nonzero value of ΔB indicates a persistent magnetic field inside the aluminum container oriented in the xy plane. We note the value of ΔB is independent of $|B_x|$, obtained by further measurements, as shown in Fig. 4. Therefore, ΔB must correspond to a remanent ferromagnetic moment in the alloy. In contrast, to within the line width, $\nu_{\rm H}$ does not depend on the orientation of the PEEK container; therefore, no ferromagnetic behavior is apparent.

While pure aluminum is paramagnetic[34], the ferromagnetism in Al-6082 could result from its alloyed elements (e.g. Fe, Cr, Mn) or contamination of the container during fabrication. To test the latter, three sample vessels were machined from a single 12.7 mm diameter rod of the

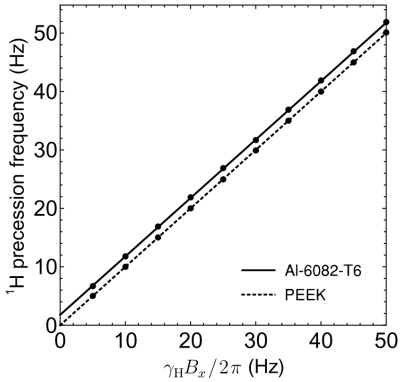

FIG. 4. Total magnetic field detected by ^{1}H NMR of water inside the PEEK/aluminum container vs. applied magnetic field B_x. The graph represents the near-zero-field part of the magnetic hysteresis curve, where the value of the vertical axis at $B_x = 0$ may be used to infer the remanent magnetization of the material.

same stock material (die-extruded Al-6082-T6 rod) using non-ferrous cutting tools. The vessels were then thoroughly washed using soap and distilled water to eliminate surface contaminants. The NMR experiment yielded the same value of ΔB within measurement error for all three copies of the container. It is therefore unlikely that the magnetization was acquired during the machining process, and is more likely a composition effect arising before or during die-extrusion of the rod.

Next we consider the ultralow-field NMR of a system where the fluid phase is dispersed in a highly porous, paramagnetic matrix. Industry-scale chemical syntheses often employ fine dispersions of catalytic metals or metal oxides on an inert porous matrix with high surface area-to-volume ratio. The intrinsically heterogeneous and disordered structure of these catalyst materials present a challenge for conventional NMR techniques when the metal is paramagnetic, since induced magnetic field gradients can arise and broaden the resonance line[35,36].

In the case of paramagnetic metal-loaded porous materials, the detection of NMR signals at ultralow field minimizes the line broadening due to gradients induced in the applied magnetic field. The effect can be demonstrated with a model system of cobalt oxide on porous silica. The material was prepared by imbibing an aqueous cobalt-(II) nitrate solution into porous silica (Fuji Silysia CARiACT^{TM} Q–50, 1.7–2.0 mm diameter spherical pellets, 50 nm mean pore diameter), oven drying at 120 °C for 12 h and then calcining at 450 °C for 1 h. The material was then imbibed in liquid decane (n-$C_{10}H_{22}$) for 12 h. Finally, after removing excess liquid the solid was flame-sealed inside a glass vial (12 mm outer diameter, 11 mm inner diameter). The setup in Fig. 1 was used to record the ^{1}H NMR spectra of the imbibed decane at B_x = 0.587 μT (25.0 Hz). Fig. 5a shows the spectra for Co loadings of 0 %, 1 % and 15 % by weight of final pellet.

The ^{1}H NMR line width (0.7 Hz full width at half maximum, FWHM) and center frequency (25.0 Hz) were both independent of the metal loading, indicating that the broadening due to paramagnetism of the material is negligible, even in the 15 wt.% sample. The line shape also proves that there is virtually no ferromagnetic moment. A nonzero ferromagnetic moment would cause the line to be broadened, or the center frequency to be shifted, upon changing the metal concentration.

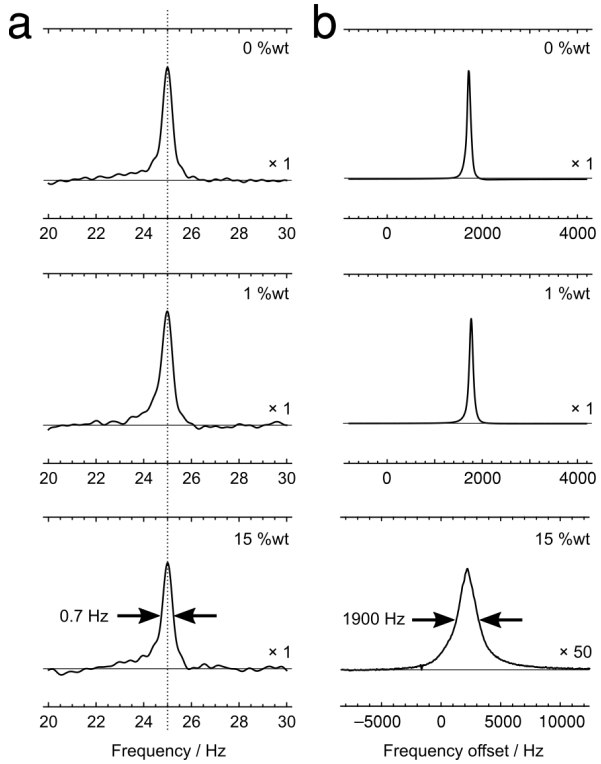

FIG. 5. The ^{1}H NMR spectra of n-decane imbibed into cobalt (II/III)-doped porous silica: (a) detected in a field of B_x = 0.587 μT, sum of 64 scans; (b) detected at 1.4 T in a commercial NMR instrument, single scans. Cobalt loading is given as percentage weight of the final material (wt.%)

For comparison, ^{1}H NMR spectra of the same samples were obtained using a commercial NMR spectrometer operating at a field of ∼1.4 T (Pulsar^{TM}, Oxford Instruments, 5 mm diameter sample tubes, ^{1}H Larmor frequency 60 MHz). Prior to the measurements the magnetic field of the 1.4 T spectrometer was made uniform to within 25 parts per billion, by a shimming procedure on the ^{1}H spectral line (12% tetramethylsilane in chloroform-d, ∼3 Hz FWHM). As Fig. 5b shows, a severe broadening of the ^{1}H NMR line is observed in the case of cobalt/porous silica. At 1 wt.% Co loading the line width is around 90 Hz (1.5 ppm), increasing to around 1900 Hz (30 ppm) for the 15 wt.% Co loading. Almost all of the line width in the NMR spectra at 1.4 T is attributed to magnetic field gradients arising within the porous material. Further measurements of natural coherence lifetime for ^{1}H precession (T_2, Carr-Purcell-Meiboom-Gibb (CPMG) pulse sequence) show that for decane in the 15 wt.% sample, a value $T_2 = (0.25 \pm 0.02)$ s was measured.

Therefore only $1/(\pi T_2) = (1.3 \pm 0.1)$ Hz of the line width is due to lifetime broadening.

The above demonstrations show that weak ferromagnetism and paramagnetism in the container material can easily be distinguished via the ^{1}H Larmor frequencies in a surrounding solvent. While magnetometers have been used to study magnetism near metal surfaces[37], weak ferromagnetism in an aluminum alloy has not previously been quantified in the literature. The measurement of the pure ferromagnetic contribution by NMR is challenging at higher fields due to (i) the paramagnetic moment of the metal and (ii) a strong attenuation of NMR signals by the skin effect, resulting in a poor signal to noise ratio unless the inductive detection coil is also placed inside the container/vessel[38]. Advantageously, the only requirement of the ultralow-field NMR method is to fill the container with water (or another ^{1}H-rich liquid) and is therefore applicable even when the sample container has an unusual geometry, has tightly confined regions or is completely sealed shut. In the future, addition of field gradient coils to the apparatus and the use of spatial labeling techniques well established in Magnetic Resonance Imaging (MRI[39]) should enable a three-dimensional map of the magnetic field $\boldsymbol{\delta B}$ to be obtained. These methods could be used to identify the source of the ferromagnetic contribution in the aluminum alloy (such as after demagnetizing or remagnetizing the alloy along a known axis), as well as characterize other dilute ferromagnets with tailored three-dimensional field profiles, including a uniform field or field gradient. Such magnets have been produced using metalized thin films[40] and additive manufacturing ("3D printing") technologies[41,42]. The magnetic moment is expected to differ significantly depending on the chemical composition and manufacturing method of the alloy. For instance, the experiment was also performed with a container made from CZ121 brass alloy. No shifts in the NMR frequency were observed.

It is noted that the spectra in Fig. 2b have similar integrated area in agreement with a minimal attenuation of the signal through metal, since the expected skin depth at the NMR frequency is around 1 cm. Similar integrated intensities were found for Al containers made with a base thickness of 1 mm or 3 mm. The broader NMR line for H_2O in the aluminum enclosure, however, corresponds to a shorter decoherence time $T_2^* = 1/(\pi \times \mathrm{FWHM})$. This may result due to gradients in the field produced by the container or an accelerated spin relaxation rate T_2. The T_1 buildup of ^{1}H magnetization in the 20 mT polarization field can provide information to deduce the mechanism. In the present case, as shown in Fig. 6, the polarization buildup time T_1 is independent of container material supporting the hypothesis that the relatively short T_2^* is due to a spatial dependence of the field contributing to ΔB. The difference in FWHM for the two spectra in Fig. 2b, $\delta\nu \approx 0.4$ Hz, provides an estimate of the inhomogeneity in the aluminum container: $\gamma_{\mathrm{H}}\delta\nu/(2\Delta B) \approx 10$ %. Furthermore, Fig. 6 shows that the NMR frequency is independent of polarizing time; this justifies the assumption that effect of the prepolarizing field (>10 mT) on the container magnetization is negligible.

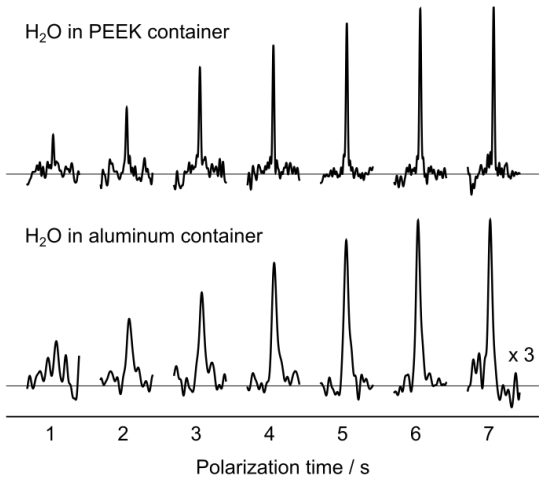

FIG. 6. ^{1}H NMR signal amplitude versus prepolarization time, showing buildup of longitudinal nuclear magnetization at the ∼20 mT polarizing field.

The case of meso-porous confinement is analogous to that of macroscopic enclosure, except that the dominant magnetic effect was the paramagnetism of the cobalt oxide. This effect led to a significant line broadening at high fields in all porous oxides tested. Even at low metal loadings (1 wt.% Co) a FWHM of 90 Hz at 1.4 T was observed, which is sufficient to prevent almost all chemical shift resolution. As the metal loading was increased towards loadings representative of industrial catalyst materials, the FWHM increased to 1.9 kHz and chemical shift resolution would have become impossible. The line broadening corresponds to a mean field of ±15 ppm times 1.4 T. In contrast, the ultralow-field NMR spectra did not incur line broadening even in the case of a 15 wt.% metal loading. Spin-spin J couplings would allow spectral resolution and therefore analysis of multiple liquid or reaction mixtures imbibed within the silica,[43,44] which is currently not feasible using high-field NMR instruments. Furthermore, the short T_2^* times exhibited at 1.4 T complicate the accurate implementation of even simple NMR pulse sequences. Sequences of multiple pulses are required to measure tortuosity, molecular diffusion and other parameters associated with molecular transport inside porous matrices, but large magnetic gradients may attenuate signals and/or distort values of parameters obtained. These effects are not an issue at ultralow fields and therefore NMR presents several opportunities for studying chemical mixtures in the proximity of highly paramagnetic materials.

In summary, ^{1}H NMR in magnetic fields of ∼1 μT has been used to study liquids in proximity to magnetic solids, including bulk metal and metal-containing porous materials. The widths of the spectral lines are narrow enough to discern, via small frequency shifts, nanotesla

magnetic fields experienced by the NMR system due to ferromagnetism of the solid, while induced line broadening does not obscure chemical resolution.

ACKNOWLEDGEMENT

The authors gratefully acknowledge Royal Dutch Shell Plc. for funding.

REFERENCES

[1]R. A. de Graaf, *In vivo NMR spectroscopy: principles and techniques*, Wiley-Interscience, 2nd edn. (2007), ISBN: 978-0470026700.
[2]J. H. Strange, L. Betteridge and M. J. D. Mallett, Characterization of porous materials by NMR, in: J. Fraissard, O. Lapina (Eds.), Magnetic Resonance in Colloid and Interface Science, NATO Science Series II, vol. 76, Springer, Dordrecht, 2002.
[3]P. F. New, B. R. Rosen, T. J. Brady, F. S. Buonanno, J. P. Kistler, C. T. Burt, W. S. Hinshaw, J. H. Newhouse and G. M. Taveras, *Radiology* 147, 139 (1983).
[4]F. D. Doty, G. Entzminger and Y. A. Yang, *Conc. Magn. Reson.* 10, 133 (1998).
[5]J. F. Schenck, *Med. Phys.* 23, 815 (1996).
[6]K. Lüdeke, P. Röschmann and R. Tischler, *Magn. Reson. Imag.* 3, 329 (1985).
[7]R. McDermott, A. H. Trabesinger, M. Mück, E. L. Hahn and A. Pines, *Science* 295, 2247 (2002).
[8]H. A. Wheeler, *Proc. IRE* 30, 412 (1942).
[9]E. C. Jordan, Electromagnetic Waves and Radiating Systems, (1968) Prentice Hall, ISBN 978-0-13-249995-8
[10]S. Xu, E. Harel, D. J. Michalak, C. W. Crawford, D. Budker and A. Pines, *J. Magn. Reson. Imag.* 28, 1299 (2008).
[11]S. Xu, V. Y. Yashchuk, M. H. Donaldson, S. M. Rochester, D. Budker and A. Pines, *Proc. Natl. Acad. Sci. USA* 103, 12668 (2008).
[12]E. O. Fridjonsson, P. L. Stanwix and M. L. Johns, *J. Magn. Reson.* 245, 110 (2014).
[13]M. Mößle, S.-I. Han, W. R. Myers, S.-K. Lee, N. Kelso, M. Hatridge, A. Pinesand J. Clarke, *J. Magn. Reson.* 179, 146 (2006).
[14]M. D. Pinter, T. Harter, M. J. McCarthy and M. P. Augustine, *MDPI Sensors* 14, 4167 (2014).
[15]Y. S. Greenberg, *Rev. Mod. Phys.* 70, 175 (1998).
[16]A. N. Matlachov, P. L. Volegov, M. Espy, J. S. George and R. H. Kraus Jr., *J. Magn. Reson.* 170, 1 (2004).
[17]L. J. Friedman, A. K. M. Wennberg, S. N. Ytterboe and H. M. Bozler, *Rev. Sci. Instrum.* 57, 410 (1986).
[18]L. Q. Qiu, Y. Zhang, H. J. Krause, A. I. Braginski, S. Tanaka and A. Offenhausser, *IEEE Transactions on Applied Superconductivity*, 19, 831, (2009).
[19]N. Q. Fan, M. B. Heaney, J. Clarke, D. Newitt, L. L. Wald, E. L. Hahn, A. Bielecki and A. Pines, *IEEE Trans. Magn.* 25, 1193 (1989).
[20]M. P. Augustine, D. M. TonThat and J. Clarke, *Solid State NMR* 11, 139 (1998).
[21]L. Trahms, and M. Burghoff, *Magn. Reson. Imag.* 28, 1244 (2010).
[22]J. Clarke, M. Hatridge, and M. Mößle, *Annu. Rev. Biomed. Eng.* 9, 389 (2007).
[23]D. Budker, and M. V. Romalis, *Nat. Phys.* 3, 227 (2007).
[24]I. M. Savukov and M. V. Romalis, *Phys. Rev. Lett.* 94, 123001 (2005).
[25]I. M. Savukov, S. J. Seltzer and M. V. Romalis, *J. Magn. Reson.* 185, 214 (2007).
[26]G. Bevilacqua, V. Biancalana, Y. Dancheva and L. Moi, *J. Magn. Reson.* 201, 222 (2009).
[27]M. C. D. Tayler, T. Theis, T. F. Sjolander, J. W. Blanchard, A. Kentner, S. Pustelny, A. Pines and D. Budker, *Rev. Sci. Instrum.* 88, 091101 (2017).
[28]M. Jiang, R. Picazo Frutos, T. Wu, J. W. Blanchard, X. Peng and D. Budker, *Phys. Rev. Appl.* 11, 024005 (2019).
[29]Y. Shimizu, J. W. Blanchard, S. Pustelny, G. Saielli, A. Bagno, M. P. Ledbetter, D. Budker and A. Pines, *J. Magn. Reson.* 250, 1 (2015).
[30]G. Bevilacqua, V. Biancalana, Y. Dancheva, L. Stiaccini and A. Vigilante, *Rev. Sci. Instrum.* 90, 046106 (2019).
[31]B. Chun, M. Jiang, Y. Ji, J. Bian, W. Xu, W. Zhang and X. Peng, *Chinese J. Lasers* 44, 1004001 (2017).
[32]I. M. Savukov, Spin Exchange Relaxation Free (SERF) Magnetometers. In: Grosz A., Haji-Sheikh M., Mukhopadhyay S. (eds) *Smart Sensors, Measurement and Instrumentation*, Springer book series, vol 19. (2016) 451-491.
[33]M. Packard and R. Varian, *Phys. Rev.* 93, 941 (1954).
[34]CRC Handbook of Chemistry and Physics, 99$^{\text{th}}$ edition, Ed J. R. Rumble, ISBN: 978-1-1385-6163-2
[35]A. J. Sederman, M. D. Mantle, C. P. Dunckley, Z. Huang and L. F. Gladden, *Catalysis Lett.* 103, 1 (2005).
[36]C. D'Agostino, M.R. Ferviour, G.L. Brett, J. Mitchell, A.P.E. York, G.J. Hutchings, M.D. Mantle and L.F. Gladden, *Catal. Sci. Technol.* 6, 7896 (2016).
[37]M. V. Romalis and H. B. Dang, *Mat. Today* 14, 258 (2011).
[38]H. Han and B. J. Balcom, *Meas. Sci. Technol.* 21, 103001 (2010).
[39]R. H. Kraus Jr., M. Espy, P. Magnelind, and P. Vogelov, *Ultra-low-field nuclear magnetic resonance: a new MRI regime*, Oxford University Press, New York (2014).
[40]A. Jesmanowicz, V. Roopchansingh, R. W. Cox, P. Starewicz, W. F. B. Punchard, J. Hyde, *Proc.* 9$^{\text{th}}$ *Scientific Meeting of the Intl. Soc. Magn. Reson. Med.*, Glasgow, Scotland, p.617 (2001).
[41]C. Huber, C. Abert, F. Bruckner, M. Groenefeld, S. Schnuschnigg, I. Teliban, C. Vogler, G. Wautlischer, R. Windl and D. Suess, *Sci. Rep.* 7, 9419 (2017).
[42]C. Huber, M. Goertler, C. Abert, F. Bruckner, M. Groenefeld, I. Teliban and D. Suess, *Sci. Rep.* 8, 14651 (2018).
[43]M. C. D. Tayler, J. Ward-Williams and L. F. Gladden, *J. Magn. Reson.* 297, 1 (2018).
[44]T. Theis, J. W. Blanchard, M. Butler, M. P. Ledbetter, D. Budker and A. Pines, *Chem. Phys. Lett.* 580, 160-165 (2013).